2015-01-2538

Modelling and evaluation of aircraft contrails for 4-Dimensional Trajectory Optimisation

Yixiang Lim, Alessandro Gardi, Roberto Sabatini
RMIT University – SAMME, Melbourne, Australia

Abstract

Contrails and aircraft-induced cirrus clouds are reputed being the largest components of aviation-induced global warming, even greater than carbon dioxide (CO_2) exhaust emissions by aircraft. This article presents a contrail model algorithm specifically developed to be integrated within a multi-objective flight trajectory optimization software framework. The purpose of the algorithm is to supply to the optimizer a measure of the estimated radiative forcing from the contrails generated by the aircraft while flying a specific trajectory. In order to determine the precise measure, a comprehensive model is employed exploiting the Schmidt-Appleman criterion and ice-supersaturation regions. Additional parameters such as the solar zenith angle, contrail lifetime and spread are also considered. The optimization of flight trajectories encompassing such contrail model allows for selective avoidance of the positive radiative forcing conditions, such as only avoiding persistent contrails, or contrails which lead to negative radiative forcing. The model assesses the radiative forcing associated with 4-Dimensional (4D) trajectories in a 4D weather field, encompassing both the local time-of-day and the contrail lifetime. Some preliminary algorithm validation activities are presented, including a simulation case study involving a medium-range domestic flight of a turbofan aircraft from Melbourne to Brisbane.

Introduction

With the currently foreseen growth of air traffic globally, the effects of aircraft condensation trails (contrails) are predicted to become significant by 2050. Currently, the physics behind the formation of contrails is relatively well understood. However, research regarding the persistence or dissipation timescales of contrails is still ongoing, with particular focus on their evolution into cirrus clouds, since these clouds have been shown to contribute significantly to global warming. The transition into cirrus is a combination of the macro-physical processes such as wind shear (which increase contrail spread), and the microphysics such as the ageing and growth of the ice particles. Contrail-based trajectory optimization is a relatively recent field of research, and work done so far has focused mainly on contrail avoidance. A review [1] noted that a general reduction in flight altitudes might not be the most effective solution due to the geographical, seasonal and diurnal variations in contrail formation regions. For example, contrails are avoided in the tropical regions by flying at a lower altitude while an increase in flight altitudes in temperate regions is required for contrail avoidance. Alternative solutions, such as shifting the air traffic densities towards sunrise and sunset, when the cooling effect of contrails is the strongest, have been suggested in other studies [2, 3]. A 4D-trajectory optimization models for contrail avoidance has been developed by [4]. This model designates persistent contrail regions as regions that both satisfy the Schmidt-Appleman criterion and are supersaturated with respect to ice, and subsequently a contrail formation cost is associated with such a region. However, not all persistent contrail regions should be penalized, as the radiative impact is also dependent on the time of day and geographic location of the contrail regions. A new scheme is presented in this paper that uses existing contrail models to compute the associated Radiative Forcing (RF) based on a set of weather, aircraft and trajectory inputs and attempts to address any possible implications arising from the adoption of such a comprehensive system. The model is specifically designed to be integrated in a Multi-Objective Trajectory Optimization (MOTO) software framework, also under development. The MOTO software is conceived for the implementation in ground-based and airborne Air Traffic Management (ATM) and Avionics systems currently under development as part of this research [5-9], addressing the strategic and tactical online operations. The contrail model will be exploited both as stand-alone and within the MOTO software to determine and optimize the formation, persistency and radiative contribution of contrails by a number of simulated flights under different weather conditions at various times of the day. Some results are included, compared and discussed here, with particular focus on the trade-offs between the environmental impact of aircraft emissions and contrail formation.

Physics of Contrail Formation

Contrails, or condensation trails, are formed from the condensation of water vapor in the plume of a jet engine and can be the precursor to the ice clouds called cirrus, found at higher altitudes where ice supersaturation is present. The formation of these contrails is thermodynamically triggered by the engine exhaust, which contains heat, moisture and soot. The contrail lifecycle is broken down into three phases: the jet, vortex and dispersion phases. The jet phase lasts for around 20 seconds and determines the thermodynamic formation of the contrail as the hot humid exhaust plume interacts and cools in the ambient air. The Schmidt-Appleman criterion, developed first by Schmidt (1941) then independently by Appleman (1953), is used to determine the onset of contrail formation [10]. The vortex phase follows from the jet phase and has a timescale of 2 minutes. In the vortex phase, the exhaust plume comes under the influence of the vortices generated by the aircraft, which causes a downward sinking of the contrails. The initial characteristics of the contrail (its breath, depth, ice properties, etc) can be considered to have stabilized and should be determined. A parametric model developed by [11] is used to model this phase. The dispersion phase follows from the end of the vortex phase and involves the advection, spread and eventual evaporation of the contrail. Depending on ambient conditions, this

can range from a few minutes, up to hours. The integration scheme employed in [11] is adapted for use in this model, with some changes. Instead of a second-order two-step Runge-Kutta scheme, a forward Euler method is used to determine the advection of the contrail. In addition, while the terminal particle velocity V_T in the former is determined as in [12], this paper uses a simplified model as in [13]. These models are developed and implemented in Matlab, with separate functions to model each phase of the contrail lifecycle.

Weather Data Retrieval

Weather data is obtained from the Global Forecasting System (GFS). Forecast data is given in a 0.25° resolution, updated 4 times daily (every 6 hours), and provides a projection of up to 180 hours in 3-hour intervals. The data is further interpolated to get a better resolution in space and time. The relative humidity with respect to ice (RHi), obtained as a function of the relative humidity with respect to water RH_w, and temperature T, both obtained from GFS

$$RH_i = RH_w \frac{p_{liq}(T)}{p_{ice}(T)} \tag{1}$$

where e_W and e_I are the saturation pressures for water vapor and ice respectively, based on empirical relations by (Sonntag 1996).

$$p_{liq}(T) = 100\exp\left[\frac{-6096.9385}{T} + 16.635794 - 0.02711193T + 1.673952e^{-5}T^2 + 2.433502\ln(T)\right] \tag{2}$$

$$p_{ice}(T) = 100\exp\left[\frac{-6024.5282}{T} + 24.7219 + 0.10613868T - 1.3198825e^{-5}T^2 - 0.49382577\ln(T)\right] \tag{3}$$

with T in degrees Kelvin.

Contrail Model

The contrail model is based on the Contrail Cirrus Prediction Tool (CoCiP) developed by Schumann [11]. The algorithm proceeds as follows. An initial check based on the Schmidt-Appleman Criterion is done to flag contrail formation segments along the flight path. A contrail lifetime analysis is then run for flagged segments. The initial size and properties of the plume are computed using a parametric model for the jet and vortex phases. These are then integrated in time using another parametric model for the dispersion phase. A model based on [14] then estimates the contrail-related RF based on the solar zenith angle, the spread and the lifetime of the contrail. A block-diagram of the algorithm is represented in Fig. 1. In the operational concept depicted in Fig. 2, an aircraft undertakes a 2-hour journey, departing at 1700hrs and arriving at 1900hrs. It encounters two contrail formation regions, shown in blue. In the first region, the contrail quickly dissipates while persistence is observed in the second region. Midway during the flight, the sun sets. The sunset line is shown as a dashed-line and subsequent contrails after this are greyed out. The model computes the RF of the second contrail and flags to the 4DT optimizer the red-shaded areas above the threshold RF, marked as a dot-dashed line.

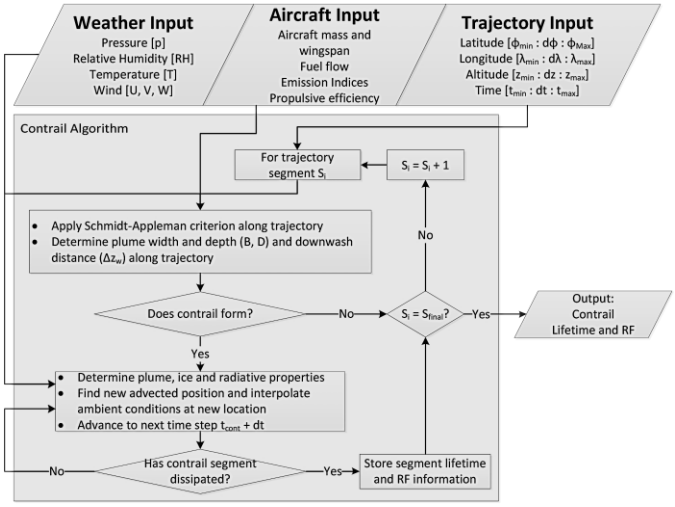

Figure 1: Block diagram of the contrail model software algorithm.

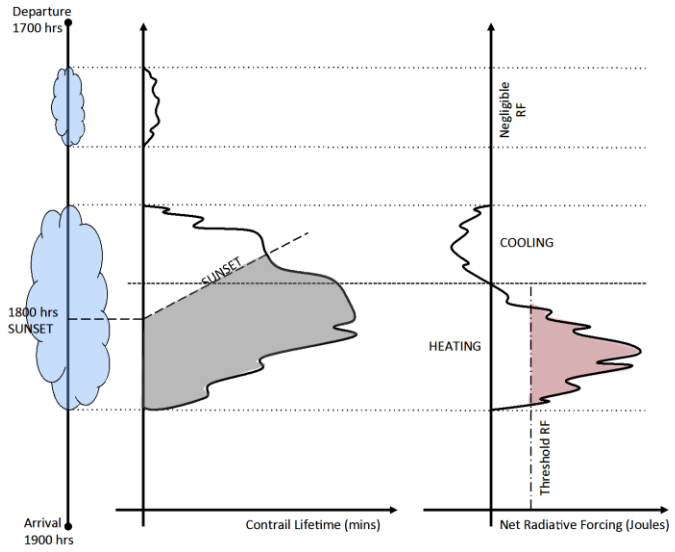

Figure 2: Operational concept of the contrail model. The timeline on the left represents the aircraft flight path. The middle graph represents the contrail lifetime and the graph on the right represents the net RF. Depending on the time of day, the RF can be positive or negative.

Jet Phase

In the jet phase, the Schmidt-Appleman Criterion is used to determine the onset of contrail formation. This is given by

$$G = \frac{EI_{H2O} \cdot c_p \cdot p}{\varepsilon \cdot Q \cdot (1-\eta)} \tag{4}$$

where G is the slope of the mixing line, in Pa K^{-1}, and describes the mixing of the exhaust plume with ambient air. EI_{H2O}, Q and η are the emission index of water vapor, heat per mass of fuel and propulsive efficiency respectively and are engine characteristics, p is the ambient pressure, and c_p and ε are the specific heat capacity of air and the ratio of the molecular masses of water and air respectively.

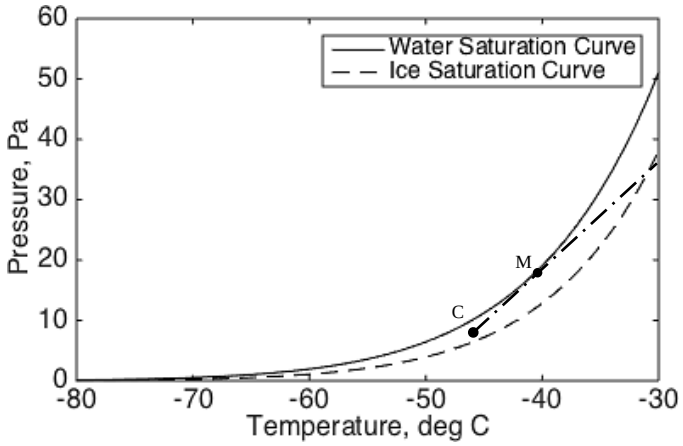

Figure 3: Mixing diagram

As the plume cools and mixes, it moves along the mixing line, as shown in Figure 3, from the top right to the bottom left, terminating at ambient conditions (Point C). The threshold conditions for contrail formation occur at Point M, where the mixing line touches the water saturation curve. Larger values of G will result in a steeper slope, leading to condensation of the exhaust plume as it crosses the water saturation curve and the formation of contrails. If ambient conditions are supersaturated with respect to ice, that is, if Point C is above the ice saturation curve, the condensed vapor will freeze into ice crystals, and the contrail might grow into cirrus given sufficient time. Reference [11] gives an approximation for the temperature at the threshold point:

$$T_{LM} = -46.46 + 9.43\ln(G - 0.053) + 0.72[\ln(G - 0.053)]^2 \quad (5)$$

in degrees celcius, where the subscript L denotes the threshold temperature for liquid saturation.

The critical temperature at ambient conditions (Point C) can then be found using the criterion given by [11] based on curve fitting where T and T_{LM} are given in degrees celcius

$$T_{LC} = T_{LM} - (1 - RH_w)\frac{p_{liq}(T_{LM})}{G} - \Delta T_C \quad (6)$$

$$\Delta T_C = F_1 RH_w[W - F_2(1 - W)] \quad (7)$$

$$W = \left(1 - RH_w{}^2\right)^{x_2} \quad (8)$$

$$F_1 = x_1 + x_3\ln(G), \qquad F_2 = \left[\frac{1}{4} - \left(RH_w - \frac{1}{2}\right)^2\right]^4 \quad (9)$$

Where $x_1 = 5.686$, $x_2 = 0.3840$, $x_3 = 0.6594$. The criterion for contrail formation is thus

$$dT = T - T_{LC} < 0 \quad (10)$$

Vortex Phase

The parametric model developed by [11] was used to estimate the initial depth and width of the contrail. This is done by first computing the maximum downward displacement Δz_w and then scaling it to obtain the initial depth. The initial width is then parameterized from the depth, dilution and fuel flow. The parameters that determine the initial size of the contrail are:

Wake vortex separation $b_0 = \pi S_a/4$,

Initial circulation $\Gamma_0 = 4M_a\, g/(\pi S_a \rho_{air} V_a)$,

Effective time scale $t_0 = 2\pi\, {b_0}^2/\Gamma_0$,

Initial velocity scale $w_0 = \Gamma_0/(2\pi b_0)$,

Normalized dissipation rate $\epsilon* = (\epsilon b_0)^{1/3}/w_0$.

These are dependent on the inputs

Wing span S_a,

Aircraft mass M_a,

True air speed V_a,

Air density ρ_{air},

Brunt Vaisaila frequency N_{BV},

Turbulent kinetic energy dissipation rate ϵ.

Schumann's parameterization distinguishes between strongly and weakly stably stratified conditions. If $N_{BV}t_0 \geq 0.8$:

$$\Delta z_w = 1.49\frac{w_0}{N_{BV}} \quad (11)$$

else, with $\epsilon* \leq 0.36$:

$$\frac{\Delta z_w}{b_0} = 7.68(1 - 4.07\,\epsilon* + 5.67\,\epsilon*^2)(0.79 - N_{BV}t_0) + 1.88 \quad (12)$$

with Δz_w as the maximum sinking.

The initial downward displacement is set to

$$\Delta z_1 = C_{z1}\Delta z_w, \qquad C_{z1} = 0.25 \quad (13)$$

where the subscript 1 denotes the end of the vortex phase. The initial depth is set to

$$D_1 = C_{D0}\Delta z_w, \qquad C_{D0} = 0.5 \quad (14)$$

and the initial width is

$$B_1 = N_{dil}(t_0)\, m_F/[(\pi/4)\rho D_1] \quad (15)$$

with the m_F being the fuel flow in kg m^{-1} and the dilution N_{dil} of the wake vortex formation being

$$N_{dil}(t) \approx 7000(t/t_s)^{0.8} \quad (16)$$

with t_s = *1s*. The initial mass mixing ratio of ice *I* and the ice particle number *N* are also prescribed for the vortex phase.

$$I_1 = I_0 - \Delta I_{ad} \quad (17)$$

$$I_0 = \frac{EI_{H2O}m_F}{(\pi/4)\rho D_1 B_1} + q_0 - q_s(p_0, T_0) \quad (18)$$

$$\Delta I_{ad} = \frac{R_0}{R_1}\left[\frac{p_{ice}(T_0 + \Delta T_{ad})}{p_1} - \frac{p_{ice}(T_0)}{p_0}\right] \quad (19)$$

Here, q_0 is the specific humidity of ambient conditions at stage "0" (the start of the vortex phase) and q_s is the specific humidity at saturation point. p_1 is the ambient pressure at stage "1", R_0 and R_1 are the specific heat capacities of air and water respectively, and

$$\Delta T_{ad} = T_0\left(R_0/c_p\right)(p_1 - p_0)/p_0 \tag{20}$$

The ice number N1 at the end of the vortex phase is determined by the soot index and a survival factor based on the ice mass ratio.

$$\mathrm{N}_1 = f_{surv} N_0 \tag{21}$$

$$N_0 = EI_{Soot} m_F, \qquad f_{surv} = \frac{I_1}{I_0} \tag{22}$$

Dispersion Phase

The state of each contrail segment along the flight path evolves with time and is described by the state vector X, denoted as $X(Position, Ambient, Plume, Particle)$ – its position in space and time, the relevant ambient conditions, and its plume and ice particle properties. The position at time t is given as

$$X.Position = (x(t), y(t), z(t), t) \tag{23}$$

where x, y and z gives the longitude, latitude and altitude of the contrail. The advection of the contrail with time is described by

$$x(t + \Delta t) = x(t) + U(t)\Delta t \tag{24}$$

$$y(t + \Delta t) = y(t) + V(t)\Delta t \tag{25}$$

$$z(t + \Delta t) = z(t) + W(t)\Delta t \tag{26}$$

with the absolute distances converted to geodetic coordinates based on approximations provided by [15]. The ambient conditions include the parameters

$$X.Ambient = (p, T, \rho_{air}, q_a, q_s) \tag{27}$$

which are pressure, temperature, density, and ambient and saturation specific humidity respectively, obtained from the GFS, and are functions of $X.Position$. The plume parameters consist of

$$X.Plume = \left(\sigma, B, D, D_{eff}, A, L, M, I, N, n, M_{H2O}, D_H, D_V\right)$$

Respectively, these are the:

Covariance matrix σ,
Contrail width B,
Contrail depth D,
Effective depth D_{eff},
Contrail area A,
Contrail length L,
Air mass M,
Ice mass mixing ratio I,
Ice particle number N,
Ice concentration n,
Water mass M_{H2O},
Horizontal diffusivity D_H,
Vertical diffusivity D_V.

The terms of the covariance matrix $\sigma = \begin{bmatrix}\sigma_{yy} & \sigma_{yz} \\ \sigma_{yz} & \sigma_{zz}\end{bmatrix}$ are initially given as

$$\sigma_{yy}(t = t_0) = B^2/8 \tag{28}$$

$$\sigma_{zz}(t = t_0) = D^2/8 \tag{29}$$

$$\sigma_{yz}(t = t_0) = 0 \tag{30}$$

and evolve with time as

$$\begin{aligned}\sigma_{yy}(t + \Delta t) = \Big[&\frac{2}{3}S^2 D_V \Delta t^3 + (S^2\sigma_{zz}(t) + 2D_S S)\Delta t^2 \\ &+ 2\left(D_H + S\sigma_{yz}(t)\right)\Delta t + \sigma_{yy}(t)\Big] \\ &\cdot \left[\frac{L(t)}{L(t + \Delta t)}\right]^2\end{aligned} \tag{31}$$

$$\sigma_{zz}(t + \Delta t) = 2D_V \Delta t + \sigma_{zz}(t) \tag{32}$$

$$\begin{aligned}\sigma_{yz}(t + \Delta t) = &\left[SD_V \Delta t^2 + \left(2D_S + S\sigma_{zz}(t)\right)\Delta t + \sigma_{yz}(t)\right] \\ &\cdot \left[\frac{L(t)}{L(t + \Delta t)}\right]\end{aligned} \tag{33}$$

with the shear diffusivity D_S set to 0 and the vertical shear of the plume normal velocity S is taken to be the total shear $S_T = \sqrt{\left(\frac{\partial U}{\partial z}\right)^2 + \left(\frac{\partial V}{\partial z}\right)^2}$. The shape and size of the contrail are based on the covariance matrix:

$$B(t + \Delta t) = \sqrt{8\sigma_{yy}(t + \Delta t)} \tag{34}$$

$$D(t + \Delta t) = \sqrt{8\sigma_{zz}(t + \Delta t)} \tag{35}$$

$$\begin{aligned}A(t + \Delta t) = 2\pi\Big\{&\frac{1}{3}S^2 D_V^2 (\Delta t)^4 + \frac{2}{3}S^2 D_V \sigma_{zz}(t)(\Delta t)^3 \\ &+ [2S\sigma_{zz}(t)(D_V - D_S) \\ &- 4(D_H D_V - D_S^2)](\Delta t)^2 \\ &+ \left[2\sigma_{zz}(t)(D_V + D_H) - 4D_S\sigma_{yz}(t)\right]\Delta t \\ &+ \sigma_{yy}(t)\sigma_{zz}(t) - \sigma_{yz}^2(t)\Big\}^{1/2}\end{aligned} \tag{36}$$

$$D_{eff}(t + \Delta t) = \frac{A(t + \Delta t)}{B(t + \Delta t)} \tag{37}$$

and the length $L(t + \Delta t)$is computed from the positions of the end-points of the contrail $x(t + \Delta t)$ and $y(t + \Delta t)$ in its position vector. The mass properties of the plume can then be calculated:

$$M(\mathrm{t} + \Delta t) = \rho A L|_{t+\Delta t} \tag{38}$$

$$I(t + \Delta t) = \frac{M(t) \cdot [I(t) + q_s(t) + \Delta M \cdot q_a]}{M(t + \Delta t)} - q_s(t + \Delta t) \tag{39}$$

$$M_{H2O}(t + \Delta t) = M(t + \Delta t) \cdot (I + q)|_{t+\Delta t} \tag{40}$$

where $\Delta M = M(t + \Delta t) - M(t)$ and $q_a = \frac{q_a(t+\Delta t)+q_a(t)}{2}$

Particle loss due to turbulence and aggregration are modelled to determine the evolution of the ice number, with the adjustable parameters E_A and E_T set to 2:

$$(dN/dt)_{agg} = -E_A\, 8\pi r_{eff}^2 V_T N^2/A \tag{41}$$

$$(dN/dt)_{turb} = -E_T\left(\frac{D_H}{\max(B, D)^2} + \frac{D_V}{D_{eff}^2}\right)N \tag{42}$$

$$\alpha = -\frac{1}{N^2}(\partial N/\partial t)_{agg}, \qquad \beta = -\frac{1}{N}(\partial N/\partial t)_{turb} \tag{43}$$

$$\mathrm{N}(t+\Delta t)=\frac{N(t)\beta\exp(-\beta\Delta t)}{\beta+N(t)\alpha[1-\exp(-\beta\Delta t)]}\frac{L(t)}{L(t+\Delta t)} \tag{44}$$

where V_T, following Rogers, 1976 (referenced in [13]), is stored in the particle properties

$$X.Particle=\left(V_T,r_{eff}\right) \tag{45}$$

$$V_T=\begin{cases}k_1r_{eff}^2, & r<40\mu m\\ k_2r_{eff}, & 40\mu m<r<600\mu m\\ k_3\sqrt{r_{eff}}, & r>600\mu m\end{cases} \tag{46}$$

$$k_1=1.9e^8, k_2=8e^3, k_3=2.2e^2\sqrt{\frac{\rho_0}{\rho}} \tag{47}$$

and r_{eff} is taken to be the effective particle radius,

$$r_{eff}=\left(\frac{\rho_{air}I}{n\rho_{ice}4\pi/3}\right)^{1/3} \tag{48}$$

Finally, the diffusivities are given in [11]

$$D_H=C_H(D^2S_T),\qquad C_H=0.1 \tag{49}$$

$$D_V=\frac{C_V}{N_{BV}}w_n'+f_t\left(V_TD_{eff}\right),\quad C_V=0.2, w_n'=0.1, f_t=0.1 \tag{50}$$

The time integration ends when the ice concentration *n* falls below 10^3 m^{-3} (or 1 l^{-1}), the ice mass ratio *I* falls below 10^{-8} (or 10^{-2} *mg/kg*), or when the time exceeds a given threshold, set to 5 *h* in this case.

Radiative Forcing

The RF model follows [14]. The parameterization scheme is based on a number of parameters that model the particle type (i.e. spherical, hollow, rosette, plate) as well as independent properties. The longwave radiation is positive and dependent on the following independent properties: the outgoing longwave radiation (OLR, W m^{-2}), the atmospheric temperature (T, K), the optical depths of the contrail and its overhead cirrus at 550 nm (τ and τ_c) and the effective particle radius (r_{eff}, μm). The contrail optical depth is computed from [11] as follows:

$$\tau=\beta D_{eff} \tag{51}$$

$$\beta=3Q_{ext}\rho I/\left(4\rho_{ice}r_{eff}\right) \tag{52}$$

$$D_{eff}=A/B \tag{53}$$

$$Q_{ext}=2-(4/\rho_\lambda)\frac{\sin(\rho_\lambda)-[1-\cos(\rho_\lambda)]}{\rho_\lambda} \tag{54}$$

$$\rho_\lambda=4\pi r_{eff}\,(\kappa-1)/\lambda,\qquad \kappa=1.31,\qquad \lambda=550nm \tag{55}$$

While the optical depth of overhead cirrus is assumed to be $\tau_c=0$. The zenith angle is approximated with ESRL's equations:

$$\gamma=\frac{2\pi}{365}*\left(day\ of\ year-1+\frac{hour-12}{24}\right) \tag{56}$$

$$\begin{aligned}eqtime=299.18[&7.5e^{-5}\\&+1.868e^{-3}\cos(\gamma)\\&-3.2077e^{-2}\sin(\gamma)\\&-1.4615e^{-2}\cos(2\gamma)\\&-0.40849e^{-2}\sin(2\gamma)]\end{aligned} \tag{57}$$

$$\begin{aligned}decl=[&6.918e^{-3}-3.99912e^{-1}\cos(\gamma)+7.026e^{-2}\sin(\gamma)\\&-6.758e^{-3}\cos(2\gamma)+9.07e^{-4}\sin(2\gamma)\\&-2.70e^{-3}\cos(3\gamma)+1.48e^{-3}\sin(3\gamma)]\end{aligned} \tag{58}$$

$$time\ offset=eqtime-4*long+60*timezone \tag{59}$$

$$tst=hour*60+min+\frac{sec}{60}+time\ offset \tag{60}$$

$$ha=\left(\frac{tst}{4}\right)-180 \tag{61}$$

$$\begin{aligned}\mu=\cos(\theta)=&\sin(lat)\sin(decl)\\&+\cos(lat)\cos(decl)\cos(ha)\end{aligned} \tag{62}$$

The long and short wave RF can then be computed.

$$\begin{aligned}\mathrm{RF}_{LW}=&[OLR-k_T(T-T_0)]\\&\cdot\left\{1-\exp\left[-\delta_\tau F_{LW}\left(r_{eff}\right)\tau\right]\right\}E_{LW}(\tau_c)\end{aligned} \tag{63}$$

$$F_{LW}\left(r_{eff}\right)=1-\exp\left(-\delta_{lr}r_{eff}\right) \tag{64}$$

$$E_{LW}(\tau_c)=\exp(-\delta_{lc}\tau_c) \tag{65}$$

The shortwave radiation is negative and depends on the following independent properties: τ, τ_c, r_{eff}, the cosine of the solar zenith angle $\mu=\cos(\theta)$, and the effective albedo (A_{eff}).

$$\mathrm{RF}_{SW}=-SDR\left(t_A-A_{eff}\right)^2\alpha_c\left(\mu,\tau,r_{eff}\right)E_{SW}(\mu,\tau_c) \tag{66}$$

$$\alpha_c\left(\mu,\tau,r_{eff}\right)=R_C\left(\tau_{eff}\right)\left[C_\mu+A_\mu R_c'(\tau')F_\mu(\mu)\right] \tag{67}$$

$$\tau'=\tau F_{SW}\left(r_{eff}\right),\qquad \tau_{eff}=\tau'/\mu \tag{68}$$

$$F_{SW}\left(r_{eff}\right)=1-F_r\left[1-\exp\left(-\delta_{sr}r_{eff}\right)\right] \tag{69}$$

$$R_C\left(\tau_{eff}\right)=1-\exp\left(-\Gamma\tau_{eff}\right),\quad R_C\left(\tau_{eff}\right)=1-\exp\left(-\gamma\tau_{eff}\right), \tag{70}$$

$$F_\mu(\mu)=\frac{(1-\mu)^{B_\mu}}{(1/2)^{B_\mu}}-1 \tag{71}$$

$$E_{SW}(\mu,\tau_c)=\exp\left(-\delta_{sc}\tau_c-\delta_{sc}'\tau_{c,eff}\right) \tag{72}$$

$$\tau_{c,eff}=\tau_c/\mu \tag{73}$$

The model parameters can be found in [14]; for this paper, a droxtal habit is assumed.

Algorithm Verification

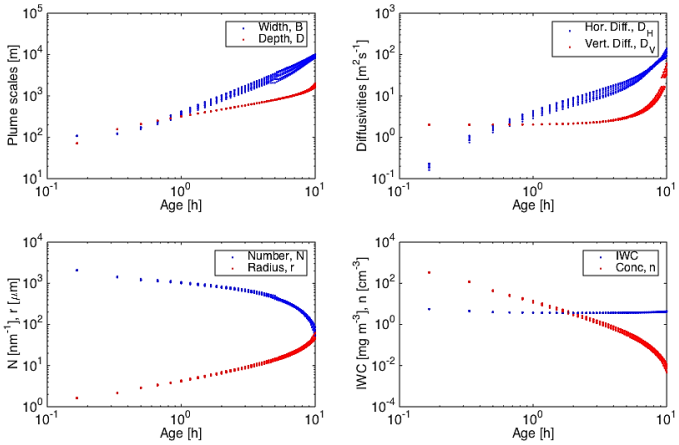

Figure 4: Contrail properties versus age, for comparison against Schuman's [11][11][11][16] results. Top-left panel: Width B and depth D. Top-right: Horizontal and vertical diffusivities. Bottom-left: Total number of ice particles per nanometer flight distance N, ice particle volume mean radius r. Bottom-right: Ice particle number concentration per volume n, ice water content per volume ρI.

For validation, results from the contrail model were compared with [11], which modeled an artificial, long lived contrail (up to 10h age) in uniform atmospheric conditions. For the purposes of comparison, a uniform RH_i and temperature field of 120% and 217K was artificially created. The properties of a few contrail segments were captured in Figure 4 and currently show good agreement with the data presented in [11].

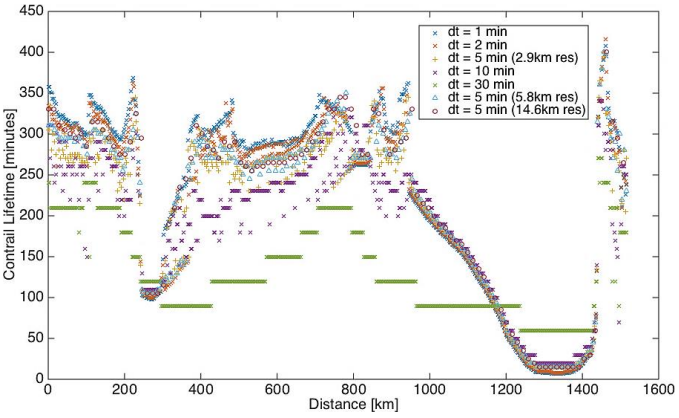

Figure 5: Contrail lifetime for the same trajectory and ambient conditions, at different time steps of 1 min (blue x's), 2 min (red x's), 5 min (orange +'s), 10 min (purple x's) and 30 min (green x's), and different grid resolutions of 5.8 km (blue triangles) and 14.6 km (purple circles) at a time-step of 5 min.

Refinement tests were conducted on the algorithm to investigate the impact of varying the time step and grid resolution. The differences in contrail lifetime for a given flight ('Scenario O' in Table 2) are presented in Figure 5 and the algorithm run time is shown in Table 1.

Table 1: Timed results of refinement test

Time step	**Mean resolution**	**Algorithm run-time**
1 min	2.9 km	1142.9 sec
2 min	2.9 km	525.7 sec
5 min	2.9 km	194.3 sec
10 min	2.9 km	89.1 sec
30 min	2.9 km	21.7 sec
5 min	5.8 km	100.6 sec
5 min	14.6 km	41.8 sec

The authors note that the validation activities are still ongoing and will lead to improved and extended results for the final submission.

Multi-objective trajectory optimization

A novel method has been developed to map the contrail region for the purposes of multi-objective trajectory optimization. Iso-persistence regions are mapped by computing the lifetime of contrails along simulated trajectories that branch out from the flight path. These trajectories are constant in time and can be imagined to be an instantaneous flight path. The combined trajectories can be interpolated to map out a 2-dimensional region of contrail lifetime like that in Figure 6. The algorithm can be run at different time-frames and at different altitudes to obtain a fully 4-dimensional, time varying volume of iso-persistence. The mapping reveals contrail persistence regions along a large part of the flight path from Stockholm to Venice. The region is closely correlated to ambient temperature and RHi variations, and roughly follows the ice super-saturation contour in Figure 6.

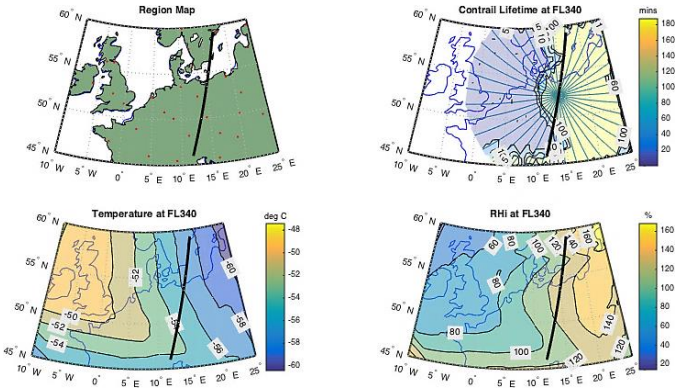

Figure 6: Flight from Stockholm to Venice (top left); iso-persistence regions (top right) are mapped along the main flight path (black line) using simulated trajectories (blue lines) at trajectory time $t = 0$, with the contrail lifetime integrated at a time-step of $dt = 2min$. Iso-persistence is closely correlated to ambient temperature (bottom left) and RH_i (bottom right).

To check the robustness of the interpolation method, contour maps interpolated with only the 'odd' and 'even' trajectories were compared with the contour map interpolated with all trajectories. These showed good agreement with one another. As the weather data was limited to $45°N < lat < 60°N$, $-10°E < long < 25°E$, the contour plots in Figure 7 and Figure 8 show a contrail lifetime of *0 min* outside the given geographical range.

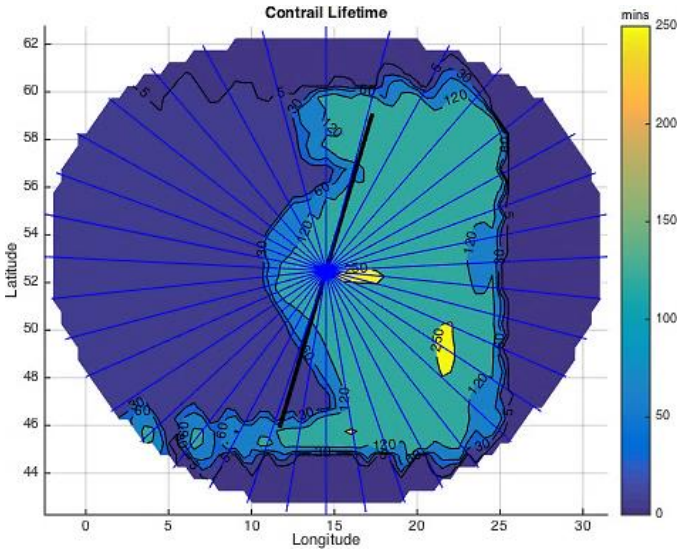

Figure 7: A zoomed-in plot of the iso-persistence region with lifetimes of (0, 1, 5, 30, 60, 120 and 250) minutes. The simulated trajectories are spaced in 10° intervals, originating from the midpoint of the flight path.

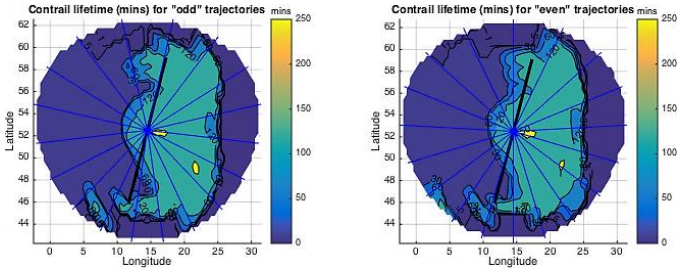

Figure 8: Contour maps which are interpolated from different trajectories, for validation purposes. The left plot shows 'odd' trajectories and the right plot shows 'even' trajectories. Both generate similar regions to the 'fully interpolated' map as shown in Figure 7.

Simulation Case Study: Re-routing

A preliminary simulation case was developed to verify the effectiveness and the computational performances of the contrail model algorithm, run for a flight from Stockholm to Venice; the flight details, along with the parameters of the simulated aircraft, are presented in Table 2 and Table 3. This simulation case study involves a constant straight and level trajectory between the Standard Instrument Departure (SID) route exit point, which is assumed to be coincident with the Top-of-Climb (ToC), and the Standard Terminal Arrival Route (STAR) entry point, which is assumed to be coincident with the Top-of-Descent (ToD). The case study examines 2 different scenarios (A and B) in comparison to the baseline (O) scenario. Scenario A involves a straight level flight at a lower altitude while Scenario B involves a bypass of the contrail persistent region at the original altitude. The temperature and RH_i fields are shown in Figure 9 for the two flight levels. The flight path as specified in scenario B is also shown in the figure. The flight takes place at night so that only the longwave radiative forcing is taken into account (shortwave forcing is zero at night).

Table 2: Details of the simulated flight

Flight Details			
Origin	Stockholm Arlanda (59.1°N, 17.3°E)		
Destination	Venice Tessera (45.9°N, 11.7°E)		
Scenario	O	A	B
Cruise Flight Path	NOSLI ROKIB	NOSLI ROKIB	NOSLI Elbe VOR Trasadingen VOR ROKIB
Altitude	FL340	FL320	FL340
Date	11 Apr 2015	11 Apr 2015	11 Apr 2015
Flight time	0000 to 0240	0000 to 0240	0000 to 0305
Net RF	6.8 mW/m^2	7.2 mW/m^2	4.9 mW/m^2

Table 3: Aircraft parameters used for the simulation

Aircraft Parameters	
Aircraft Model	Airbus A320
Wingspan, S_a	34.1 m
Mass, M_a	64 000 Kg
True Airspeed (TAS) in cruise, V_a	236.8 m s^{-1}
Fuel flow, m_F	0.17 kg s^{-1}
Soot number per fuel mass, EI_{soot}	2.8 10^{14} kg^{-1}
Emission Index for water, EI_{H2O}	1.23
Fuel combustion heat, Q_{fuel}	43.2 MJ kg-^{1}
Propulsion efficiency, η	0.3

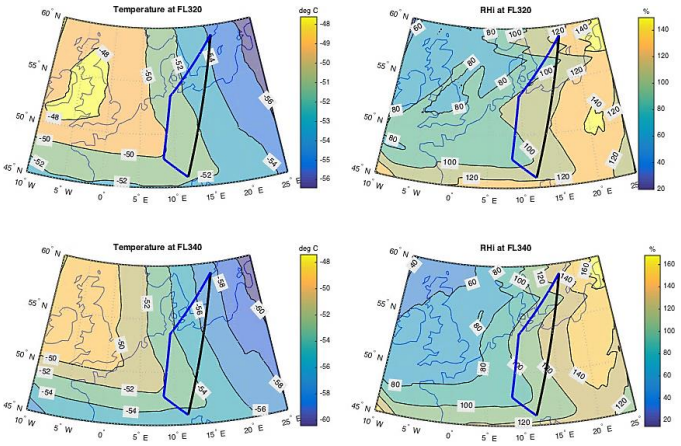

Figure 9: Contours of temperature (left) and RH_i (right) data at FL320 (top) and FL340 (bottom). The blue flight path corresponds to the deviated trajectory as per scenario B.

For the simulation, the imported weather data uses a resolution of 0.25° along isobars of 5kPa, in 3 hour intervals. This was interpolated along an altitude with resolution of 5 ft (converted from pressure isobars) in 10 min intervals. The trajectory was subdivided into

segments of mean resolution 2.9 km for analysis, and the ambient conditions were again interpolated at these points. The time integration of the contrail segments was computed with a time-step of *dt =2 min*. The results are presented in Figure 10. The plots show the evolution of contrail properties along the flight path. The contrail formation criterion is based on Equation (10), which measures the difference between ambient and threshold temperature *dT*; a more negative *dT* indicates a greater probability of contrail formation. The contrail RF and lifetime are strongly correlated to the RH_i; when the RH_i drops below 100% (ice-subsaturated) the contrail lifetime experiences a sharp drop. Even minor fluctuations in the RH_i can significantly affect the contrail lifetime. This case study indicates that a bypass might be more efficient in contrail avoidance than a general reduction in flight altitude.

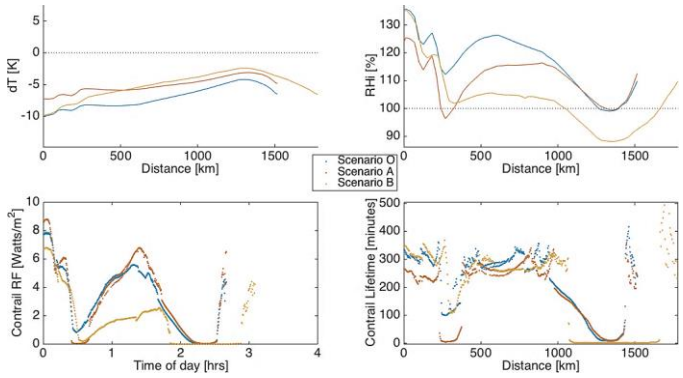

Figure 10: Plots of dT in Kelvins (top left), ambient RH_i in % (top right), contrail RF in W/m^2 (bottom left) and lifetime in minutes (bottom right) for Scenarios O (blue), A (red) and B (orange). The RF from O and A are comparable while B has significantly reduced RF.

Simulation Case Study: Trajectory Optimisation

The final verification of the contrail model was achieved upon integration into a multi-objective trajectory optimization framework. The aim of this verification case was to highlight the viability of adopting the mapped contrail iso-persistence or iso-radiative forcing region as the basis for the optimization of the flight trajectory with respect to two or more objectives. The developed contrail model is capable of providing a 4D mapping of the iso-persistence and iso-radiative forcing regions, which can be exploited for the optimization of fully 4D trajectories. Nevertheless, as the current operational approach of ATM restricts aircraft to cruise at discrete flight levels, the solution implemented in this article adopts a 2-Dimensional plus Time (2D+T) trajectory optimization approach at constant flight level. The cruise phase of an hypothetical AIRBUS A320 aircraft flying between Chicago to Quebec City at FL340 was simulated. The 2D+T iso-persistence mapping was generated for a marginally augmented search domain covering parts of the USA and Canada. The origin and destination were amended slightly such that the trajectory passed through most of the contrail region. The verification case was run with the contrail region generated using the *fmincon* optimization algorithm provided by Matlab. A cost function that included weighted penalties for both the contrail lifetime and flight time was used. Figure 11 shows the results of the 2D+T trajectory optimization.

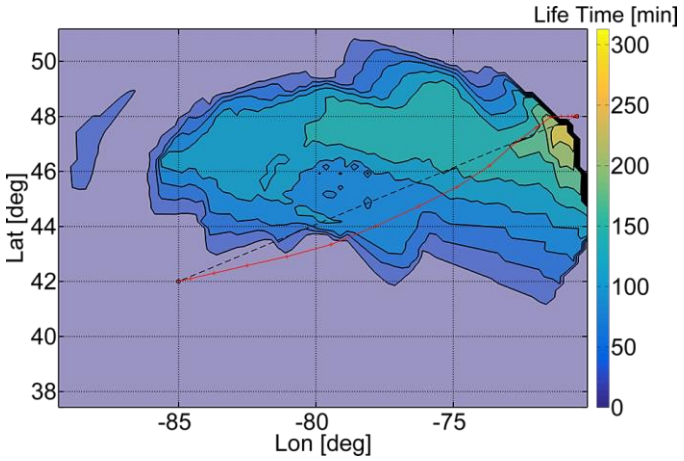

Figure 11: Optimal 2D+T trajectory at constant flight level for a given contrail 2D+T iso-persistence mapping region.

Summary

This paper presented the design and the underlying theoretical framework of a customized contrail model and the related software algorithm. The model is specifically conceived to be integrated in a Multi-Objective Trajectory Optimization (MOTO) software framework, enabling the minimization of contrail formation. More in detail, in addition to the contrail formation, the algorithm determines the lifetime and the net radiative forcing associated with the specific 4-Dimensional (4D) trajectory of an aircraft in defined space and time. For this purpose, the algorithm entails fully 4D modeling of the atmospheric thermodynamic quantities from a global weather dataset, as well as the solar zenith angle based on the time-of-day. Further research will address the exploitation of the model in a number of optimisation case studies of flight trajectories, both in the offline and in the online contexts. For this purpose, the contrail model will be integrated in the ground-based Air Traffic Management (ATM) systems and airborne Avionics also being researched at present [5-9].

Appendix

Table 4: List of parameters

Parameter	Description	Unit
Jet Phase		
G	Mixing line slope	$Pa\ K^{-1}$
EI_{H2O}	Emission Index of water	$kg\ kg^{-1}$
c_p	Specific heat capacity of air	$J(kg\ K)^{-1}$
p, p_{liq}, p_{ice}	Ambient pressure, saturation pressures of water and ice	Pa
ε	Ratio of molecular masses of water to air	1
Q	Heat of fuel combustion	$J\ kg^{-1}$
η	Propulsive efficiency	1
T, T_{LM}, T_{LC}	Ambient temperature, maximum threshold temperature, threshold temperature at ambient conditions	K

Vortex Phase		
b	Wake vortex separation	m
Γ	Wake vortex circulation	$m^2 s^{-1}$
t	Effective time scale	s
w	Vertical velocity scale	ms^{-1}
$\epsilon*$	Normalized dissipation rate	1
S_a	Wing span	m
M_a	Aircraft mass	kg
V_a	True air speed	ms^{-1}
ρ, ρ_{air}	Air density	kgm^{-3}
N_{BV}	Brunt Vaisaila frequency	s^{-1}
ϵ	Kinetic energy dissipation rate	$m^2 s^{-3}$
Δz_w	Downwash distance	m
m_F	Fuel consumption per flight distance, per flight time	kgm^{-1} kgs^{-1}
B	Contrail breadth	m
D, D_{eff}	Contrail depth and effective depth	m
N_{dil}	Ratio of contrail mass and fuel flow per length	1
I	Ice mass mixing ratio	$kgkg^{-1}$
q_a, q_s	Specific humidity at ambient and saturation conditions	$kgkg^{-1}$
R_0, R_1	Gas constants of air and water vapor	$J(kgK)^{-1}$
N	Total ice number per contrail length	m^{-1}
f_{surv}	Fraction of particles surviving the vortex phase	1
Dispersion Phase		
x, y	Longitude, latitude	$°E, °N$
z	Altitude	m, ft
t	Time	s, min
Δt	Integration time-step	s, min
U, V, W	Wind speeds in x, y, z direction	ms^{-1}
A	Contrail segment cross-section area	m^2
L	Horizontal segment length	m
M, M_{H2O}	Plume air and water mass per contrail length	kgm^{-1}
n	Ice concentration	m^{-3}
σ	Covariance matrix	m^2
$\sigma_{yy}, \sigma_{zz}, \sigma_{yz}$	Elements of σ	m^2
D_H	Horizontal diffusivity	$m^2 s^{-1}$
D_V	Vertical diffusivity	$m^2 s^{-1}$
S, S_T	Plume normal shear, total shear	s^{-1}
E_A	Particle loss aggregation parameter	1
E_T	Particle loss turbulence parameter	1
V_T	Particle terminal velocity	ms^{-1}
r_{eff}	Particle effective radius	m
ρ_{ice}	Ice density	kgm^{-3}
Radiative Forcing		
RF_{LW}, RF_{SW}	Long and shortwave radiative forcing	Wm^{-2}
OLR	Outgoing longwave radiation	Wm^{-2}
SDR	Solar direct radiation	Wm^{-2}
β	Optical extinction	m^{-1}
Q_{ext}	Solar radiation extinction efficiency	1
γ	Fractional year	$rads$
$eqtime$	Equation of time	min
$decl$	Solar declination angle	$rads$
$time\ offset$	Time offset	min
$long, lat$	Longitude, latitude	$°E, °N$
$timezone$	Timezone from UTC	$hrs\ UTC$
tst	True solar time	min
ha	Solar hour angle	°
τ, τ_c	Optical depth of contrail and overhead cirrus	1
θ	Solar zenith angle	°
μ	Cosine of solar zenith angle	1
A_{eff}	Effective albedo	1

References

1. K. Gierens, L. Lim, and K. Eleftheratos, "A Review of Various Strategies for Contrail Avoidance", *The Open Atmospheric Science Journal*, vol. 2, pp. 1-7, 2008. DOI: 10.2174/1874282300802010001
2. R. Meerkötter, U. Schumann, D. R. Doelling, P. Minnis, T. Nakajima, and Y. Tsushima, "Radiative forcing by contrails", in proceedings of *Annales Geophysicae*, 1999, pp. 1080-1094. DOI: 10.1007/s00585-999-1080-7
3. G. Myhre and F. Stordal, "On the tradeoff of the solar and thermal infrared radiative impact of contrails", *Geophysical Research Letters*, vol. 28, pp. 3119-3122, 2001. DOI: 10.1029/2001gl013193
4. M. Soler, B. Zou, and M. Hansen, "Flight trajectory design in the presence of contrails: Application of a multiphase mixed-integer optimal control approach", *Transportation Research Part C: Emerging Technologies*, vol. 48, pp. 172-194, 2014. DOI: 10.1016/j.trc.2014.08.009
5. R. Sabatini, A. Gardi, S. Ramasamy, T. Kistan, and M. Marino, "Novel ATM and Avionic Systems for Environmentally Sustainable Aviation", in proceedings of *Practical Responses to Climate Change. Engineers Australia Convention 2014 (PRCC 2014)*, Melbourne, Australia, 2014. DOI: 10.13140/2.1.1938.0808

6. A. Gardi, R. Sabatini, T. Kistan, Y. Lim, and S. Ramasamy, "4-Dimensional Trajectory Functionalities for Air Traffic Management Systems", in proceedings of *Integrated Communication, Navigation and Surveillance Conference (ICNS 2015)*, Herndon, VA, USA, 2015. DOI: 10.1109/ICNSURV.2015.7121246
7. S. Ramasamy, R. Sabatini, and A. Gardi, "Novel Flight Management Systems for Improved Safety and Sustainability in the CNS+A Context", in proceedings of *Integrated Communication, Navigation and Surveillance Conference (ICNS 2015)*, Herndon, VA, USA, 2015. DOI: 10.1109/ICNSURV.2015.7121225
8. M. Marino, A. Gardi, R. Sabatini, and T. Kistan, "Multi-Objective Trajectory Optimization Concepts and Models for Implementation into the Next Generation Air Traffic Management System", *SAE Technical Paper 2015-01-2392*, 2015. DOI: 10.4271/2015-01-2392
9. A. Gardi, R. Sabatini, S. Ramasamy, M. Marino, and T. Kistan, "Automated ATM System Enabling 4DT-Based Operations", *SAE Technical Paper 2015-01-2539*, 2015. DOI: 10.4271/2015-01-2539
10. H. Appleman, "The formation of exhaust condensation trails by jet aircraft", *Bull. Amer. Meteor. Soc*, vol. 34, pp. 14-20, 1953
11. U. Schumann, "A contrail cirrus prediction model", *Geoscientific Model Development*, vol. 5, pp. 543-580, 2012. DOI: 10.5194/gmd-5-543-2012
12. I. Sölch and B. Kärcher, "A large-eddy model for cirrus clouds with explicit aerosol and ice microphysics and Lagrangian ice particle tracking", *Quarterly Journal of the Royal Meteorological Society*, vol. 136, pp. 2074-2093, 2010. DOI: 10.1002/qj.689
13. V. I. Khvorostyanov and J. A. Curry, "Terminal velocities of droplets and crystals: Power laws with continuous parameters over the size spectrum", *Journal of the atmospheric sciences*, vol. 59, pp. 1872-1884, 2002
14. U. Schumann, B. Mayer, K. Graf, and H. Mannstein, "A Parametric Radiative Forcing Model for Contrail Cirrus", *Journal of Applied Meteorology and Climatology*, vol. 51, pp. 1391-1406, 2012. DOI: 10.1175/jamc-d-11-0242.1
15. C. Veness. (2015, 25/3/2015). *Movable Type Scripts*. Available: http://www.movable-type.co.uk/scripts/latlong.html